Published as Yang et al, IEEE Sensors Journal, 10.1109/JSEN.2023.3258501, author version v1

Acoustic Flow Sensor Using a Passive Bell Transducer

Samuel K. E. Yang, Michail E. Kiziroglou, Senior Member, IEEE, Eric M. Yeatman, Fellow, IEEE and Andrew S. Holmes, Member, IEEE

***Abstract*— Sensing based on a passive transducer that is wirelessly linked to a nearby data collection node can offer an attractive solution for use in remote, inaccessible, or harsh environments. Here we report a pipe flow sensor based on this principle. A transducer mounted inside the pipe generates an acoustic signal that is picked up by an external microphone. The passive transducer comprises a cavity with a trapped ball that can oscillate in response to flow. Its collisions generate an acoustic signal correlated to the flow speed. The transducer is implemented on a 6 mm diameter probe and characterized as a water flow meter. The time - average microphone voltage output is calculated by an analogue circuit, without any further signal processing. With the microphone mounted on the probe, and for flow rates in the range 0.35 m/s to 6.5 m/s, correlation between the sensor voltage output and flow rate data from a commercial flow meter is demonstrated with a worst-case accuracy of 2%. This was achieved by simple averaging of the acoustic pulse train over a 5-second time interval. Consistent correlation with the microphone mounted on the pipe wall at distances up to 150 mm from the probe location is also reported. These results demonstrate the viability of remote acoustic flow sensing using passive structures and offer a simple and minimally invasive flow monitoring method.**

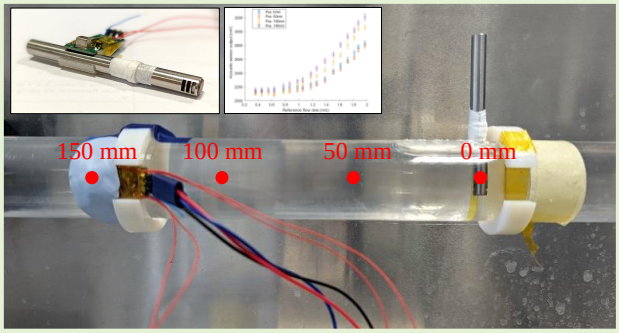

***Index Terms*— Acoustic, Energy Autonomy, Fluid Flow, Passive Sensor, Wireless**

I. Introduction

THE tremendous progress in electronic technologies related to the Internet-of-Things (IoT) in the last ten years has created widespread expectation for autonomous, deploy-and-forget wireless sensing systems. However, industrial adoption of such technologies has been slow due to power autonomy and installation limitations, especially at remote, inaccessible, or harsh environment locations. A promising approach is to use a passive device at the sensing location that transduces the quantity of interest to a signal that can be picked up wirelessly by a nearby receiver. This is illustrated in Fig. 1. This approach provides physical and electrical decoupling of the transducer from electronics, power supply, energy storage and communications, which results in several key advantages, including (i) reliable sealing; (ii) power autonomy and communication at remote, inaccessible, or RF-shielded locations; (iii) simplification of the structure required at the sensor location, which can provide new opportunities for sensing in toxic, extreme temperature, radiative and other harsh environments; (iv) ability to integrate the required passive transducer into the manufacturing process of the monitored system [1] and (v) applicability to disposable sensors, such as medical diagnostic devices, in which the low-cost passive structure may be disposed, while the separate active part may be kept for reuse.

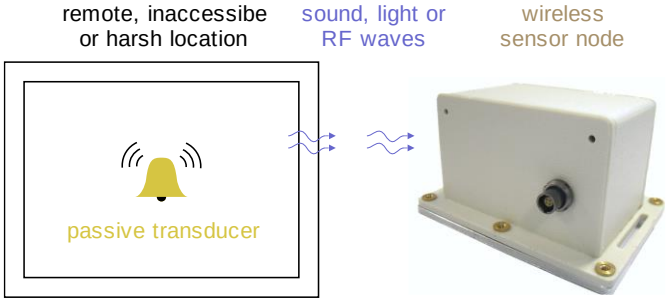

Fig. 1: Illustration of the passive remote transducer method. The indicative sensor node on the right is the autonomous strain sensor from [2].

In this work, an implementation of the passive remote transducer concept of Fig. 1 is presented. This implementation is based on a bell-like operating concept, in which a trapped ball follows an oscillatory motion due to fluid flow. The ball collisions with the walls of its enclosure create sound wave packets of frequency and attenuation that depend on wall dimensions and on fluid density and viscosity respectively. The collision rate can be correlated to the flow speed. An early report on this concept was presented in [3]. After a literature review (Section II), the concept and basic correlation demonstration using manual analysis of received acoustic signals is discussed in Section III. A new ball and cavity architecture is introduced in Section IV, integrated into the

Manuscript received Month xx, 2xxx; revised Month xx, xxxx; accepted Month x, xxxx. The authors are with the Department of Electrical and Electronic Engineering, Imperial College London, SW7 2AZ, U.K. (e-mail: m.kiziroglou@imperial.ac.uk)

M. E. Kiziroglou is also with the Department of Industrial Engineering and Management, International Hellenic University, 57400, Greece.

minimally invasive multisensor platform of [4], and including hardware-implemented signal processing. Evaluation results and conclusions are presented in Sections V and VI.

II. Literature Review

In fluid-flow monitoring, the most common invasive sensing concepts are based on turbine counters, heat dissipation probes and drag-force transducers [5, 6]. Recent research in heat-dissipation based flow meters includes miniaturization and integration into Micro-Electro-Mechanical Systems (MEMS) devices [7, 8] , improvement of accuracy, sensitivity and range as well as enhanced thermal control [9]. Inductive and piezoelectric air flow meters with power autonomy have been reported [10, 11]. A miniaturized true differential pressure flow meter has also been reported in [12]. Flow sensors developed for biomedical applications include drag-force [13], calorimetric [14] and opto-thermal [15] operating principles, with special interest in biodegradable and low-cost disposable implementations [14, 16]. A review of miniaturized flow sensors can be found in [5].

Non-invasive methods include ultrasound time-of-flight [17] and acoustic doppler effect [18] systems. Remote, passive acoustic sensor implementations have also been investigated, mainly using a vortex whistle structure [19-22]. Such a structure directs the fluid into a spiral trajectory that generates a sound wave. The frequency and intensity of sound depend on the flow rate, and thereby a measure of flow can be obtained by a remote microphone and signal processing. Vortex whistle sensors are a special case of the sensing scheme described in Fig. 1 and the proof of concept has been demonstrated for gas [19-22] as well as liquid flow [19]. A fluidic oscillation model for vortex whistle sensors has also been proposed in [20]. Other studies in this direction include the exploitation of natural flow sound [23], pipe vibration [24], as well as the speed of ambient sounds through the flowing fluid [25]. A summary of these implementations is presented in Table 1. Furthermore, flow induced vibration in general has been considered for energy harvesting [26-34], sensing [33] or both [10], typically employing active materials on the vibrating structures.

Table 1
Features Of Various Passive Acoustic Flow Sensors.

Group / Year	Fluid	Wave Generation Concept	Sensor output	Wireless Integration
Vonnegut [19], 1957	Air, Water	Vortex Whistle	48 Hz/(m/s)	No
Watanabe & Sato [20], 1994	Air	Vortex Whistle	50 Hz/(m/s)	No
Hou et al [23], 1999	Water	Flow Sound	35 V^2/Hz/(m/s)	No
Di et al [21] , 2013	Various Gasses	Vortex Whistle	24 Hz/(m/s)	No
Godin et al [25], 2014	Air	Ambient Sound	Sound speed, Not available	No
Venkata&Navada [24], 2018	Oil, Water	Pipe Vibration	10 mV/(m/s)	No
Awan & Awan [22], 2020	Air	Vortex Whistle	110 Hz/(m/s)	No
This work	Water	Bell	1.6 V / (m/s)	Yes

III. Acoustic Sensor

A. Operating Concept

The operating concept of the passive acoustic transducer involves a ball in a cavity that is driven to an oscillatory motion when fluid flow enters the inlet of the cavity as shown in Fig. 2. The oscillating ball collides with the cavity walls which produces an acoustic signal which can be correlated to the flow rate. A similar concept of flow transduction to an acoustic signal have been demonstrated in the form of a vortex whistle [19-22, 35]. In comparison to those, the ball-cavity concept reduces the complexity of the passive transducer structure. In addition, the ball-cavity collision acoustic signal can also be analyzed to extract more information on the fluid properties and the infrastructure condition.

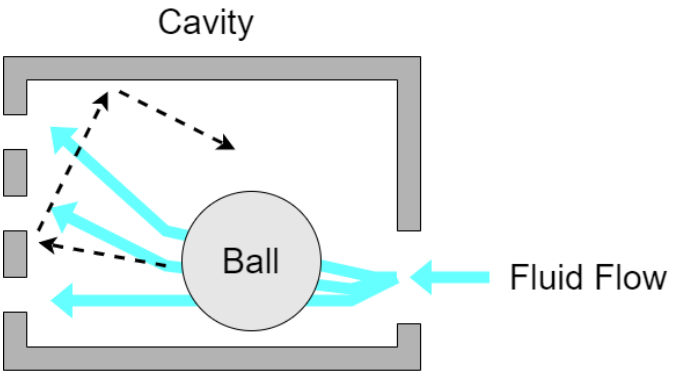

Fig. 2: Operating concept of the acoustic sensor. The cavity design and dimensions are conceptual only.

B. Proof-of-principle

In this section, a proof-of-principle implementation of a passive acoustic ball-cavity sensor is described. Fig. 3 shows a 3D-printed acoustic sensor which comprises a cavity and a 5 mm diameter plastic ball installed into it. A custom water flow testing rig is used as an evaluation platform. The flow rig includes an AM-50 water pump from Crest Pumps Ltd, a water filter and an ABB FEP611 magnetic flow meter as reference. The pipeline inner diameter of this platform is 28 mm. An InvenSense ICS-40180 microphone module [1] is mounted on the pipe wall facing the acoustic sensor. The microphone output signal is recorded using a Picoscope 2000 and further data analysis and processing is done using MATLAB.

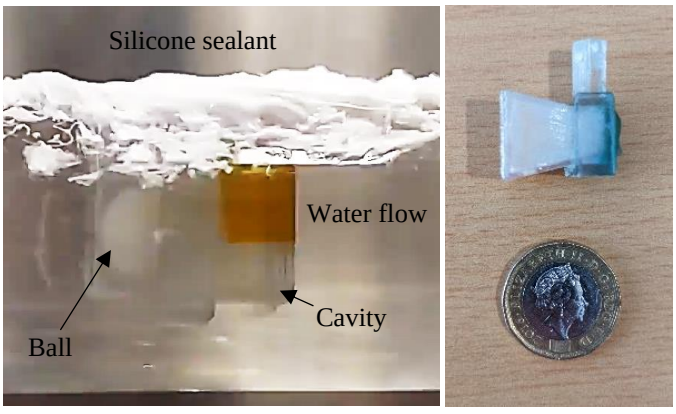

Fig. 3: Left: Ball-cavity acoustic sensor sealed in a water flow pipe. Right: Acoustic sensor size comparison with a £1 coin.

The collision between the ball and cavity produces sounds that are translated to peaks on the microphone signal. The resulting signal is rectified by a digital absolute value calculator, and divided into 5 s long intervals. Indicative such signal intervals for three different flow rate speeds are shown in Fig. 4.

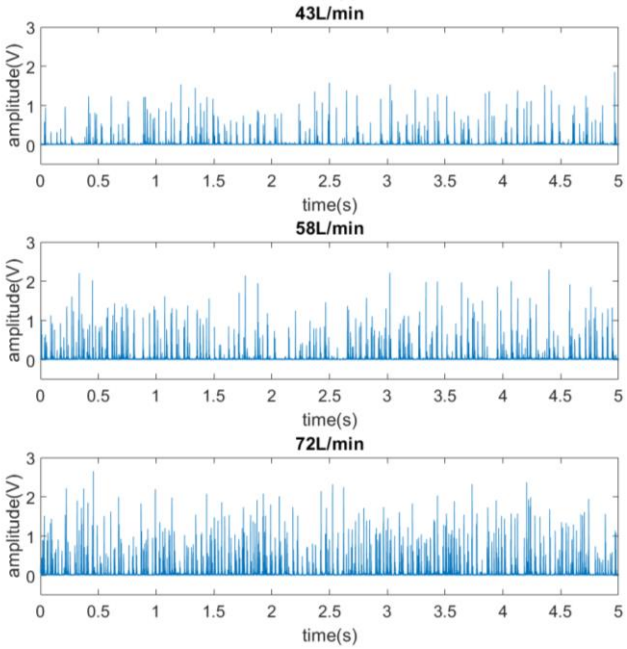

Fig. 4: Measured collision peaks corresponding to different flow rates.

It is observed that the occurrence rate and magnitude of these sound peaks, which correspond to ball-cavity hits, increases with heat flow. A clear correlation is observed by plotting the five second average of these signal samples as a function of flow rate as shown in Fig. 5. The reproducibility of the result was studied by calculating the average of sixty randomly selected 5 s interval acoustic signal samples and plotting the results in the form of error bars in Fig. 5. Further information about this implementation can be found in [1] .

The effect of ball size to the sensor performance was also evaluated in a separate experiment. Fig. 6 shows the signal average plots for balls with 5 mm, 8 mm and 11 mm diameter. Higher ball sizes result in a more intense signal and a clearer correlation.

The periodic ball motion inside the cavity is generally stochastic and its modes, along with the ball and cavity vibration modes in response to collisions, determine the acoustic signal properties. In order to gain insight on the expected ball motion trajectory in response to water flow, stationary finite element modeling simulations of water flow in the cavity structure were conducted using the COMSOL software package. The results are shown in Fig. 7. The flow speed map indicates that the water from the inlet pushes the ball upwards towards the left, resulting in collision with the left and top cavity walls. Once it reaches the upper region where flow rate is low, the ball sinks downwards due to gravity and the cycle is repeated. This ball motion prediction is in agreement with slow-motion video clips acquired during experiments, although some irregular motion events are also observable. The simulation results of Fig. 7 also indicate that the bottom inlet doesn't significantly affect the flow profile of the water inside the cavity. On the other hand, the inlet must be large enough for providing adequate lift pressure to the balls, and aligned to the outlet design such that the low flow speed region on the top right of the cavity in Fig. 7 is maintained.

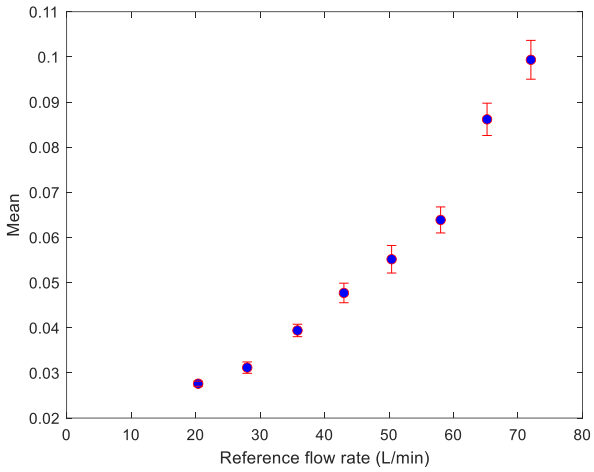

Fig. 5: Measured signal average vs reference flow rate. The error bars represent a repeatability experiment including sixty signal samples.

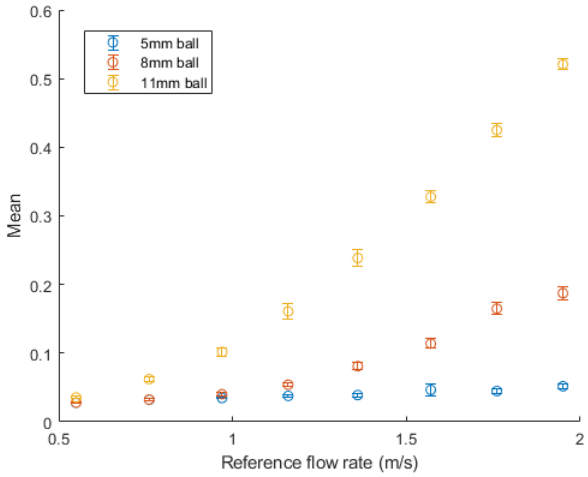

Fig. 6: Signal average vs reference flow rate, now converted to m/s for different ball sizes.

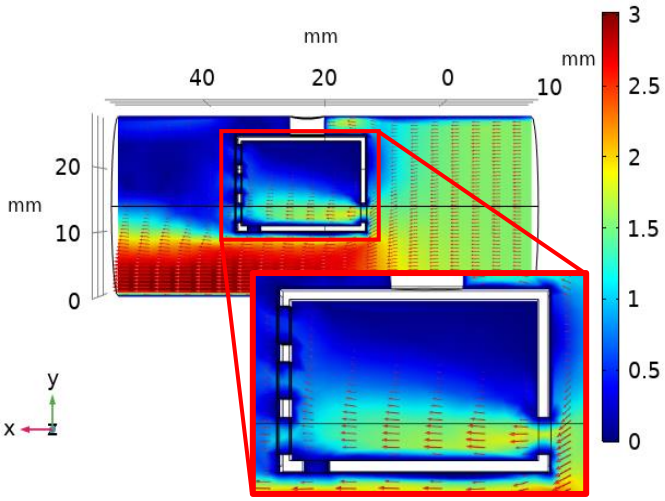

Fig. 7: Finite element modeling of water flow profile inside the cavity. Flow direction: right to left.

IV. Integrated Acoustic Sensor Probe

A. Sensor probe design

The acoustic sensor demonstrated in Section III was redesigned and scaled down to fit in a 6 mm diameter probe package. This design allowed the sensor to be integrated into the multi-sensor platform that was introduced in [4]. The scaling down of the passive structure design could also allow its integration into the manufacturing process of water pipes without occupying significant space or obstructing the flow. The sensor probe dimensions are presented in Fig. 8. It is made of stainless-steel, by conventional machining. The probe design includes a cut-out cavity at the end. The cavity accommodates two 2.5 mm-diameter Polyoxymethylene (POM) balls. POM was selected as a hard plastic commercially available in the desired form. The double-ball implementation was selected to increase the number of collision pulses. The natural beam vibration frequency of the stainless-steel probe is in the 1 kHz range for a 100 mm probe length.

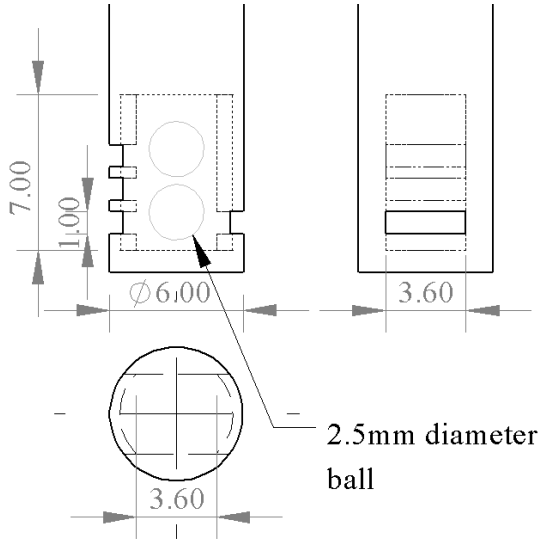

Fig. 8: Dimension of the acoustic sensor probe in mm. Top left: Sideview illustrating the one-hole inlet and the three-hole outlet on the right and left of the probe respectively. Top right: Front view illustrating the one-hole inlet. Bottom left: top view of the probe.

B. Sensor node electronics

The microphone readout board is mounted on the surface of the sensor probe and connected to a Texas Instruments CC2650 [4] Launchpad, which is a low power Bluetooth Low Energy (BLE) Micro-Controller Unit (MCU) development kit. In the performance characterization of the prototype reported in [4] the acoustic sensor output was measured and logged using an oscilloscope. In the prototype presented here, the microphone circuit has been redesigned to give an analog output that can be easily acquired by the MCU Analogue to Digital Converter (ADC) channel.

The system diagram of the sensor node electronics is shown in Fig. 9. The InvenSense ICS-40730 microphone is employed, which provides higher nominal signal-to-noise ratio (SNR) and sensitivity than the ICS-40180 used in [1]. Its frequency response range is 20 Hz – 20 kHz. This corresponds well to the ball-cavity collision sound frequency expected from the stainless-steel probe beam vibration mode, which is in the kHz range. The microphone signal is fed to an active rectifier, an amplifier with a gain of 64, a bandpass filter, and a comparator to produce a waveform of clear positive voltage pulses and reduce noise. The comparator is configured to a 0.5 V threshold. This method improves the experimental consistency and increases repeatability, at the expense of lower sensitivity and less signal information such as the oscillation frequency of the pulses. This information is not exploited in this work but could be useful in other implementations for fluid characterization and sensor state diagnosis. Subsequently, a lowpass filter based averaging circuit is used to obtain the DC average of the signal, which is further amplified and fed into an ADC channel of the MCU. An advantage of this hardware signal processing implementation is the drastic reduction of the required sampling rate, from the kHz range to 1 Hz and below, which allows duty cycling operation and reduces significantly the sensing power demand. A picture of the sensor probe is shown in Fig. 10, with the microphone frontend board mounted on it using a 3D-printed holder.

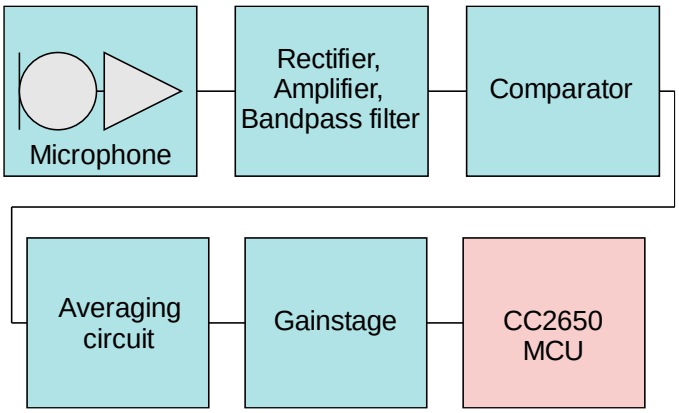

Fig. 9: System diagram of the acoustic sensor electronics.

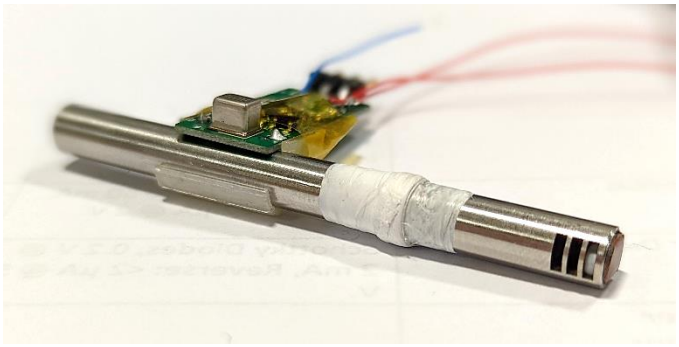

Fig. 10: Sensor node electronics mounted on the sensor probe. Two balls are installed inside the cavity at the end of the probe.

C. Experimental setup

The experimental setup used for the acoustic sensor probe characterization is shown in Fig. 11. The frontend electronics board is wired to the MCU, which receives its output signal through an ADC port. The ADC sampling rate is set to 22 kHz. The signal waveform is recorded in 1 s long intervals and the average sampled value is calculated by the MCU. For each measurement, ten such intervals are recorded and their overall average and standard deviation are calculated. The results are collected and displayed by a computer connected to the MCU through a universal serial bus (USB) interface.

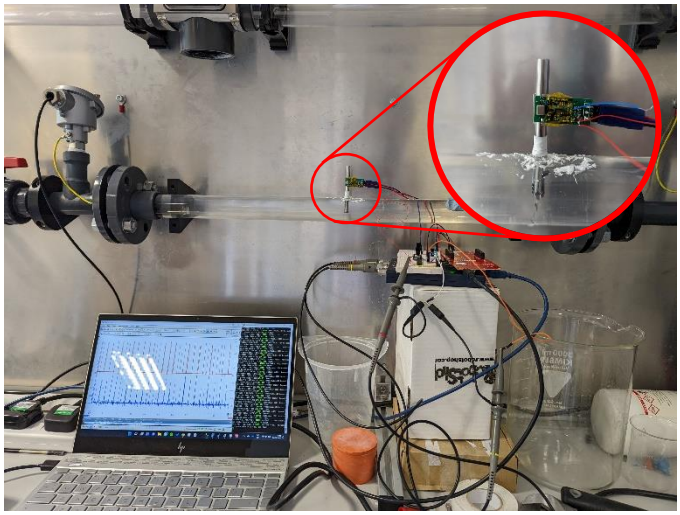

Fig. 11: Experimental setup of acoustic sensor probe on the flow rig. Microphone mounted on probe.

The 28 mm diameter test rig has a maximum flow rate of around 2 m/s. To allow testing at higher speeds, a 3D printed tube with 14 mm and 28 mm internal and external diameter respectively is inserted into the flow pipe. The smaller resulting flow cross-section area leads to velocity increase by a factor of 4. For the correlation of measurements at 14 mm diameter locations to the reference values obtained by the magnetic flow meter, which is installed at a 28 mm location, a flow value correspondence table was generated, from a finite element modeling numerical simulation study, using the COMSOL software package. An indicative simulation diagram quantifying the resulting flow rate increase is shown in Fig. 12. The maximum flow obtained by this method is 7 m/s. It is noted that for these high flow rate measurements, a reduced linearity and accuracy may be expected, as the reference values are not directly calibrated. Nevertheless, the measurement repeatability is not expected to be affected by this.

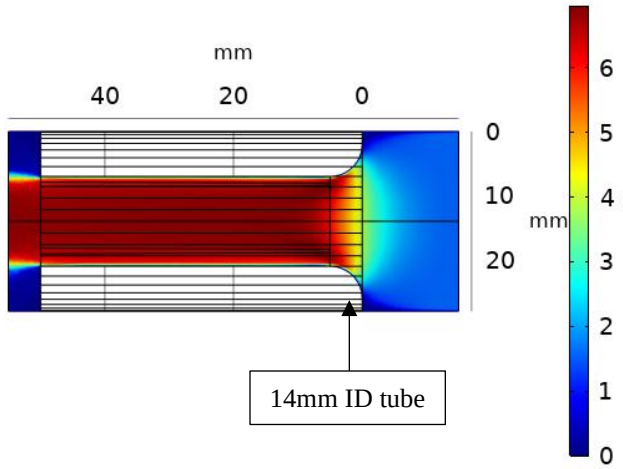

Fig. 12: Effect of printed tube to the flow profile in the pipe (length of tube and water pipe not exact). Flow direction: right to left.

Experiments with the microphone mounted directly on the outside surface of the plastic pipe walls, at distances up to 150 mm from the probe location were also performed. These experiments aim at investigating the possibility of decoupling the passive transducer from the active microphone and electronics, in order to exploit the benefits of remote passive acoustic sensing discussed in Section I of this paper. The four microphone positions used for the measurements are at 0 mm, 50 mm, 100 mm and 150 mm from the probe, as illustrated in Fig. 13.

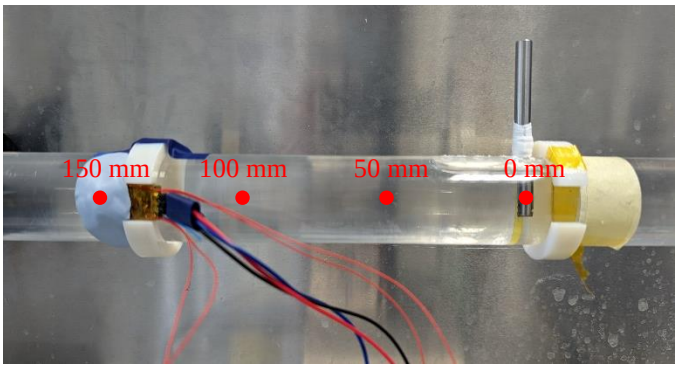

Fig. 13: Microphone pipe wall mounting positions used in the remote acoustic sensing experiments.

D. Power supply and energy management

The frontend electronics components have been selected for low power consumption in order to allow for long power autonomy of the complete system. The nominal consumption of the microphone, the amplifier employed in the amplification stages, the comparator and the regulator used as the microphone power supply are listed in Table 2. The rest of the frontend electronic components are passive. The total active-mode current consumption of the acoustic sensor frontend circuit is less than 0.5 mA and it is dominated by the microphone. At the 3.3 V voltage supply used in this work, this corresponds to 1.8 mW. The MCU current consumption is also listed in Table 2 for reference. Further power consumption reduction could be achieved by operating the microphone in a low duty cycle mode, in accordance with data acquisition requirements for a given application. This low power consumption is beneficial for the overall energy autonomy of the complete system.

TABLE 2
NOMINAL CURRENT CONSUMPTION OF DIFFERENT COMPONENTS IN THE ACOUSTIC SENSOR CIRCUIT

Function	Components	Current consumption (mA)
Microphone	InvenSense ICS-40730	0.375
Amplifier	ADA4505-2ARMZ-RL	0.007
Comparator	LTC1441	0.002
Linear voltage regulator	TI TPS76033DBVR	0.1
MCU Active	TI CC2650	1.5
MCU 0 dBm TX/RX	TI CC2650	6.1

V. Evaluation

The acoustic sensor data output measured when the microphone is mounted on the probe as a function of flow rate, up to 2 m/s, is shown in Fig. 14. For these measurements, the amplification of the final gain stage is set to 11, to increase the maximum analog output to about 3 V. Similar measurements for higher flow rates are shown in Fig. 15. These are plotted separately, as their reference flow values are extrapolated from the reference flow meter using simulation as described in Section IV.C. In addition, the final gain for these measurements is reduced to limit the voltage amplitude below the 4.3 V reference voltage of the ADC. In both cases, a good correlation between the analog output and the reference flow rate is demonstrated with low standard deviation. Results from a second, separate experimental run under the same conditions are also included in Fig. 14 and Fig. 15, indicated as test number 2, demonstrating adequate reproducibility.

A similar response is also obtained from the remote acoustic sensing experiments, with the microphone installed directly on the plastic pipe surface at the locations indicated in Fig. 13.

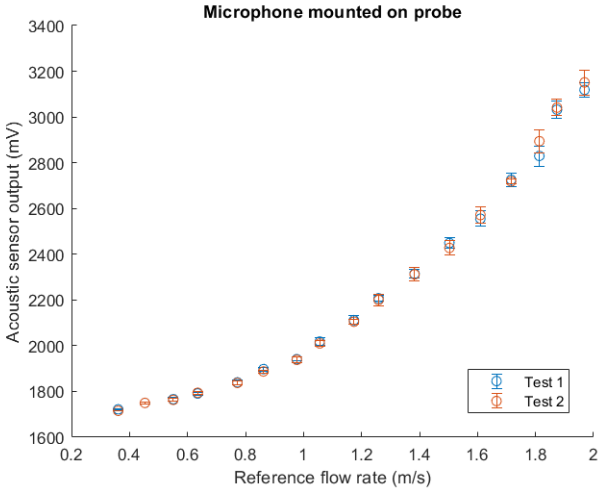

Fig. 14: Recorded sensor output as a function of flow rate, with the microphone mounted on the probe.

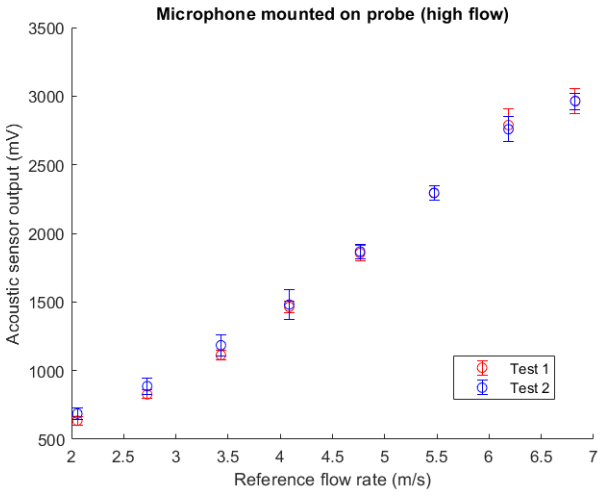

Fig. 15: Recorded sensor output for higher flow rates obtained using a 14 mm diameter pipe, with the microphone mounted on the probe. In comparison with Fig. 14, a reduced amplification gain is used to fit the MCU ADC voltage range.

The corresponding measurements are plotted in Fig. 16. As the flow rate is reduced, the sensor output levels-off earlier (below 0.7 m/s) compared to when the microphone is mounted on the probe (below 0.4 m/s). This indicates a reduction of sensitivity. This may be due to acoustic signal attenuation in the plastic pipe and in the fluid, as well as to reflections at the sound path interfaces. The experimental results show a worst-case accuracy of 2%. Sources of measurement error include acoustic noise, turbulent flow and incidental ball motion irregularities. The impact of these effect to sensor performance can be reduced by employing longer averaging intervals.

In general, the inner diameter of pipe as well as the size of the structure is expected to affect the volume of the acoustic signal. This could potentially be compensated by calibration either as part of sensor installation or dynamically during operation by adjustment according to the average amplitude of as-received individual waveforms. Electromagnetic noise is not expected to have a significant effect on the performance of this type of sensors, as its physical correlation with ball motion, cavity vibration and acoustic signal propagation is small. Temperature variation can however change the fluid density and viscosity and thereby the fluid dynamics in the cavity. To evaluate this effect, the laminar fluid flow of Fig. 7 was simulated at temperatures between 10 ºC and 80 ºC, showing velocity distribution differences below 5%, similar to the change of water density in this temperature range. On the other hand, water viscosity varies substantially, from around 1.3 $mPa \cdot s$ at 10 ºC to 0.35 $mPa \cdot s$ at 80 ºC [36], and further study of this effect is required in order to calibrate the output and evaluate the performance of the proposed sensor under large temperature fluctuations. Thermal expansion of the metal tube is expected to result in a minor shift of the acoustic signal frequency which has a negligible effect on device performance. A larger thermal expansion of the polymer balls is expected (≈ 0.01% / ºC for POM), but with a rather small volume increase and impact to fluid dynamics.

Overall, these results demonstrate that the microphone provides the best response in direct acoustic contact with the probe. At a distance, it can still provide reliable flow monitoring, although at lower sensitivity.

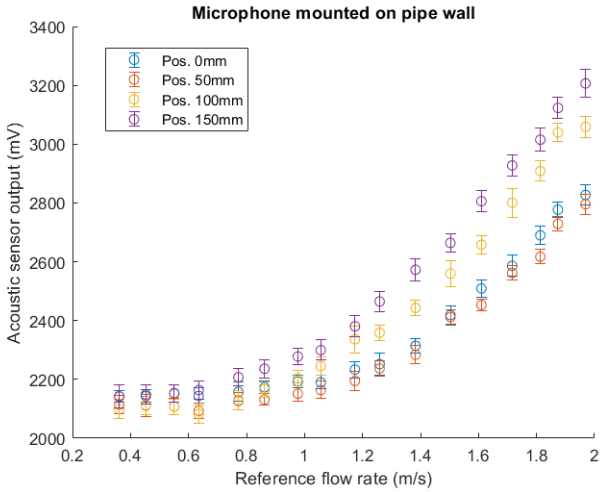

Fig. 16: Sensor plots when microphone is mounted on different positions along the pipe walls as shown in Fig. 13. Inner tube is not used to increase flow rate ranges.

As mentioned, the properties of as-received collision pulses can also be analyzed in order to obtain information about the fluid properties, the equipment and infrastructure conditions and to distinguish among acoustic collision pulses coming from different sensors. This potential has not been exploited in the experimental results presented in this section. Indicatively, three collision pulses, received by the microphone and amplified by the first amplification stage of the frontend electronics are presented in Fig. 17. Their frequency spectrum, calculated by a fast fourier transformation algorithm is shown in the inset. A first evaluation of their potential for providing a distinction signature can be obtained by calculating their frequency to bandwidth ratio:

$$Q = \frac{f}{\Delta f} \quad (1)$$

where f is the peak frequency and Δf is the 3 dB frequency bandwidth of the pulse. For the broad spectrum peak between 10 kHz and 25 kHz in the inset of Fig. 17 this ratio is around 2. Further data analysis could allow distinction among signals from different sensors, noise filtering, evaluation of fluid properties and probing the transducer condition. As an example, the precise oscillation frequency value and the pulse attenuation could be used to acquire fluid density and viscosity information, similarly to the operating principle of vibration based viscosity sensor probes.

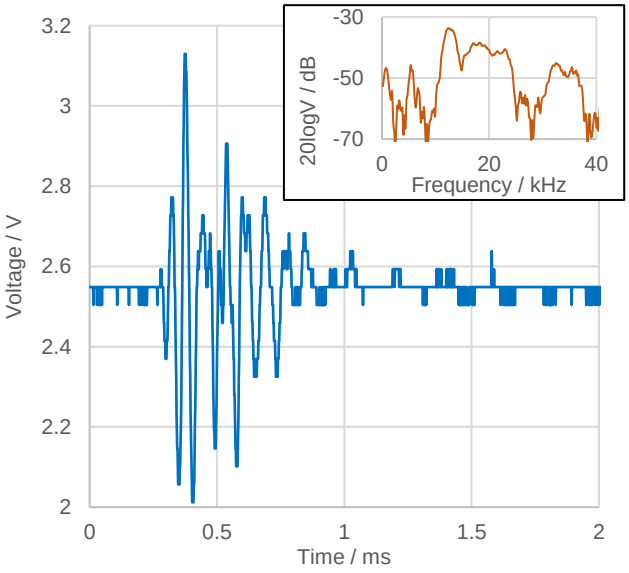

Fig. 17: An indicative collision pulse recorded by the microphone; the signal is offset to 2.5 V due to the 2.5 V amplifier bias. Its spectrum is shown in the inset.

VI. Conclusion and Outlook

The results presented in this work provide an experimental demonstration of passive acoustic flow sensing. This is achieved by a simple passive bell transducer design without structural optimization, and simple rectification and averaging signal processing. The direct and clear correlation of voltage output to the overall intensity of the acoustic signal show high potential for a new class of non-invasive flow sensors, using passive structural elements embedded in the infrastructure in combination with external, low-power wireless microphones. The passive element does not require high precision manufacturing steps or special materials, resulting in low fabrication cost. This is an important manufacturing advantage, especially for applications that benefit from disposable sensing tips such as biomedical sensors. The active electronic system also comprises wide-spread standard sensor electronics parts, resulting in lower overall system cost compared to flow sensors that require specialized active probes and front-end electronics.

The simple implementation presented here demonstrates reliable correlation for flow rates higher than 0.7 m/s, with a resolution of around 0.1 m/s, and sensitivity of 1.2 V/(m/s), with a microphone installed on the external surface of the plastic pipe and at an axial distance of 150 mm from the transducer location. This performance exceeds the current state-of-art of passive acoustic flow sensors as compared in Table 1. The advanced performance is attributed to the ball collision device concept which is strongly coupled to the flow speed and provides a distinctive acoustic signal, allowing higher signal-to-noise ratio. An additional advantage of this implementation is that it is integrated into the minimally invasive sensor platform of [4]. The development of optimized designs for the passive bell structures and the employment of advanced signal processing methods, including acoustic pattern recognition, is expected to allow resolution and accuracy improvement and extend significantly the microphone-transducer distance range. Such improvements could also allow pulse distinction for multiple passive acoustic sensors operation on the same medium. Finally, pulse waveform analysis could provide complementary information on the fluid as well as on the condition of the passive structure. For example, extraction of parameters such as the resonance frequency and attenuation factor of the received collision wave packets are expected to be correlated to the fluid density and viscosity respectively, as well as to dirt accumulation or corrosion of the passive structure. In this direction, an experimental study of received pulse waveforms under liquid flows of variable viscosity would be highly interesting.

References

[1] Invensense. (2021). *RF-Hardened, Low-Noise Microphone with Bottom Port and Analog Output*. Available: https://invensense.tdk.com/wp-content/uploads/2015/02/DS-000021-v1.22.pdf

[2] L. v. Allmen *et al.*, "Aircraft Strain WSN powered by Heat Storage Harvesting," *IEEE Transactions on Industrial Electronics,* vol. 64, no. 9, pp. 7284-7292, 2017.

[3] S. Yang, M. Kiziroglou, E. Yeatman, and A. Holmes, "Passive acoustic transducer as a fluid flow sensor," 2021. Available: http://hdl.handle.net/10044/1/91458

[4] A. S. Holmes *et al.*, "Minimally Invasive Online Water Monitor," *IEEE Internet of Things Journal,* vol. 9, no. 16, pp. 14325 - 14335, 2021.

[5] F. Ejeian *et al.*, "Design and applications of MEMS flow sensors: A review," *Sensors and Actuators A: Physical,* vol. 295, pp. 483-502, 2019/08/15/ 2019.

[6] N. T. Nguyen, "Micromachined flow sensors—a review," *Flow Measurement and Instrumentation,* vol. 8, no. 1, pp. 7-16, 1997/03/01/ 1997.

[7] E. Gardner, A. De Luca, J. Coull, C. Lee, and F. Udrea, "On the Design of the World's Smallest Flow Sensor Package," *IEEE Sensors Letters,* vol. 5, no. 6, Jun 2021, Art. no. 6500104.
[8] W. Xu, X. Y. Wang, Y. Chiu, and Y. K. E. Lee, "High Sensitivity and Wide Dynamic Range Thermoresistive Micro Calorimetric Flow Sensor With CMOS MEMS Technology," *IEEE Sensors Journal,* vol. 20, no. 8, pp. 4104-4111, Apr 2020.
[9] V. Kitsos, A. Demosthenous, and X. Liu, "A Smart Dual-Mode Calorimetric Flow Sensor," *Ieee Sensors Journal,* vol. 20, no. 3, pp. 1499-1508, Feb 2020.
[10] M. Shi, A. S. Holmes, and E. M. Yeatman, "Piezoelectric wind velocity sensor based on the variation of galloping frequency with drag force," *Applied Physics Letters,* vol. 116, no. 26, p. 264101, 2020.
[11] S. K. E. Yang, B. Chilukuri, P. Ratra, G. Lepipas, and A. S. Holmes, "Batteryless Wireless Anemometer with BLE Connectivity," in *2022 21st International Conference on Micro and Nanotechnology for Power Generation and Energy Conversion Applications (PowerMEMS)*, 2022, pp. 86-89.
[12] A. S. Holmes *et al.*, "Miniaturized Wet-Wet Differential Pressure Sensor," in *2022 IEEE Sensors*, 2022, pp. 1-4.
[13] U. Saha, A. Kamat, D. Sengupta, B. Jayawardhana, A. G. P. Kottapalli, and Ieee, "A Low-Cost Lung Monitoring Point-of-Care Device Based on a Flexible Piezoresistive Flow Sensor," in *IEEE Sensors Conference*, Electr Network, 2020, 2020.
[14] J. Kim, H. Cho, S. I. Han, A. Han, and K. H. Han, "A disposable microfluidic flow sensor with a reusable sensing substrate," *Sensors and Actuators B-Chemical,* vol. 288, pp. 147-154, Jun 2019.
[15] A. Ruiz-Vargas, S. A. Morris, R. H. Hartley, and J. W. Arkwright, "Optical flow sensor for continuous invasive measurement of blood flow velocity," *Journal of Biophotonics,* vol. 12, no. 10, Oct 2019, Art. no. e201900139.
[16] C. M. Boutry *et al.*, "Biodegradable and flexible arterial-pulse sensor for the wireless monitoring of blood flow," *Nature Biomedical Engineering,* vol. 3, no. 1, pp. 47-57, Jan 2019.
[17] Siemens. Sitrans clamp-on ultrasonic flow measurement. https://new.siemens.com/global/en/products/automation/process-instrumentation/flow-measurement/ultrasonic/clamp-on.html, 2023.
[18] (2021). *Greyline DFM 6.1 Doppler Flow Meter*. https://pulsarmeasurement.com/greyline-dfm-6-1
[19] B. Vonnegut, Vortex Whistle Measuring Instrument For Fluid Flow Rates And/Or Pressure, General Electric Co, US Patent No. US2794341A, Available: https://patents.google.com/patent/US2794341A/en, 1953.
[20] K. Watanabe and H. Sato, "Vortex whistle as a flow meter," in *Conference Proceedings. 10th Anniversary. IMTC/94. Advanced Technologies in I & M. 1994 IEEE Instrumentation and Measurement Technolgy Conference (Cat. No.94CH3424-9)*, 1994, pp. 1225-1228 vol.3.
[21] Y.-b. Di, C. Gerhardy, and W. Karl Schomburg, "Vortex whistles employed as remote micro flow sensors," *Flow Measurement and Instrumentation,* vol. 34, pp. 11-18, 2013/12/01/ 2013.
[22] S. N. Awan and J. A. Awan, "Use of a Vortex Whistle for Measures of Respiratory Capacity," *Journal of Voice,* 2020/09/09/ 2020.
[23] R. Hou, A. Hunt, and R. A. Williams, "Acoustic monitoring of pipeline flows: particulate slurries," *Powder Technology,* vol. 106, no. 1, pp. 30-36, 1999/11/22/ 1999.
[24] S. K. Venkata and B. R. Navada, "Estimation of Flow Rate Through Analysis of Pipe Vibration," *Acta Mechanica et Automatica,* vol. 12, no. 4, pp. 294-300, 2018.
[25] O. A. Godin, V. G. Irisov, and M. I. Charnotskii, "Passive acoustic measurements of wind velocity and sound speed in air," *The Journal of the Acoustical Society of America,* vol. 135, no. 2, pp. EL68-EL74, 2014.
[26] H. J. Zhu, T. Tang, H. H. Yang, J. L. Wang, J. Z. Song, and G. Peng, "The State-of-the-Art Brief Review on Piezoelectric Energy Harvesting from Flow-Induced Vibration," *Shock and Vibration,* vol. 2021, Apr 2021, Art. no. 8861821.
[27] P. Han, Q. G. Huang, G. Pan, W. Wang, T. Q. Zhang, and D. H. Qin, "Energy harvesting from flow-induced vibration of a low-mass square cylinder with different incidence angles," *Aip Advances,* vol. 11, no. 2, Feb 2021, Art. no. 025126.
[28] J. L. Wang, L. F. Geng, L. Ding, H. J. Zhu, and D. Yurchenko, "The state-of-the-art review on energy harvesting from flow-induced vibrations," *Applied Energy,* vol. 267, Jun 2020, Art. no. 114902.
[29] W. P. Sun, D. L. Zhao, T. Tan, Z. M. Yan, P. C. Guo, and X. Q. Luo, "Low velocity water flow energy harvesting using vortex induced vibration and galloping," *Applied Energy,* vol. 251, Oct 2019, Art. no. 113392.
[30] Y. J. Lee, Y. Qi, G. Zhou, and K. B. Lua, "Vortex-induced vibration wind energy harvesting by piezoelectric MEMS device in formation," *Scientific Reports,* vol. 9, no. 1, p. 20404, 2019/12/31 2019.
[31] D. Li, Y. Wu, A. Da Ronch, and J. Xiang, "Energy harvesting by means of flow-induced vibrations on aerospace vehicles," *Progress in Aerospace Sciences,* vol. 86, pp. 28-62, 2016/10/01/ 2016.
[32] D. A. Wang and H. H. Ko, "Piezoelectric energy harvesting from flow-induced vibration," *Journal of Micromechanics and Microengineering,* vol. 20, no. 2, Feb 2010, Art. no. 025019.
[33] K. H. Kim and Y. H. Seo, "Self-Resonant Flow Sensor using Resonance Frequency Shift by Flow-Induced Vibration," in *2009 IEEE 22nd International Conference on Micro Electro Mechanical Systems*, 2009, pp. 511-514.
[34] D. S. Clair, A. Bibo, V. R. Sennakesavababu, M. F. Daqaq, and G. Li, "A scalable concept for micropower generation using flow-induced self-excited oscillations," *Applied Physics Letters,* vol. 96, no. 14, p. 144103, 2010.
[35] B. Vonnegut, "A Vortex Whistle," *The Journal of the Acoustical Society of America,* vol. 26, no. 1, pp. 18-20, 1954.
[36] J. C. Crittenden, R. R. Trussell, D. W. Hand, K. J. Howe, and G. Tchobanoglous, "Appendix C: Physical Properties of Water," in *MWH's Water Treatment: Principles and Design, Third Edition*, 2012, pp. 1861-1862.